

SOLUBILITY ENHANCEMENT OF GLIBENCLAMIDE USING MESOPOROUS SILICA

SWATI MITTAL*, AKSHAY SONAWANE, MANGESH KHUNE

Department of Vivekanand Education Society's College of Pharmacy, University of Mumbai, Mumbai, Maharashtra, India.

Email: swati.mittal@ves.ac.in

Received: 17 May 2019, Revised and Accepted: 30 July 2019

ABSTRACT

Objective: Glibenclamide (GLB) is a Class II drugs encounter the problem of low solubility and low bioavailability. The rate-limiting step for absorption is low solubility, not permeation. Therefore, various approaches in drug formulation development have been used for enhancing solubility and thereby bioavailability of Biopharmaceutical Classification System Class II drugs. These techniques include solid dispersions, complexation using cyclodextrins, self-microemulsifying drug delivery system, hydrotrophy, liquisolid compacts, and adsorption on carriers such as mesoporous silica and Magnesium Aluminometasilicate. Adsorption onto mesoporous silica has demonstrated considerable potential in enhancing the solubility of poorly soluble drugs. The objective of the present study is to investigate the effect of drug adsorption on SYLOID XDP 3050 carrier complex on the dissolution of GLB tablet.

Methods: A 3² full factorial design was adopted to optimize the ratio of GLB (X1) and mesoporous silica as a carrier (X2) and the effect of different ratios was studied on percent yield, percent drug loading, and percent drug release. X-ray powder diffraction and differential scanning calorimetry studies were performed to investigate any possible interaction between GLB and mesoporous silica.

Results: Obtained results of glibenclamide tablets dissolution show that more the amount of carrier taken for adsorption more the drug release in lesser time.

Conclusion: The solubility of GLB was enhanced by loading onto SYLOID® XDP 3050 matrix. Furthermore, the dissolution profile of GLB-loaded SYLOID® XDP 3050-containing tablets was also improved as compared with conventional and commercially available GLB tablets. This study indicates that non-ordered mesoporous SYLOID® XDP 3050 is a promising carrier, which enhances the oral bioavailability of poorly water-soluble drugs.

Keywords: Glibenclamide, Solubility enhancement, Mesoporous silica, Precipitation inhibitor.

© 2019 The Authors. Published by Innovare Academic Sciences Pvt Ltd. This is an open access article under the CC BY license (<http://creativecommons.org/licenses/by/4.0/>) DOI: <http://dx.doi.org/10.22159/ajpcr.2019.v12i9.34182>

INTRODUCTION

Oral administration is the most preferred route of drug administration due to convenience, cost-effectiveness, and high patient compliance. All orally administered drugs must be solubilized in the aqueous environment of the gastrointestinal tract before absorption [1]. According to the Biopharmaceutical Classification System (BCS), Class II drugs encounter the problem of low solubility and low bioavailability [2]. The rate-limiting step for absorption is low solubility, not permeation. Therefore, various approaches in drug formulation development have been used for enhancing solubility and thereby bioavailability of BCS Class II drugs. These techniques include solid dispersions, complexation using cyclodextrins, self-microemulsifying drug delivery system, hydrotrophy, liquisolid compacts, and adsorption on carriers such as mesoporous silica and Magnesium Aluminometasilicate [3,4]. Adsorption onto mesoporous silica has demonstrated considerable potential in enhancing the solubility of poorly soluble drugs [5]. The drugs can exist in an amorphous or molecularly dispersed state on the surface of mesoporous silica, thus displaying higher apparent solubility and dissolution compared to the crystalline substance [6,7].

Supersaturation is one of the prominent strategies to enhance intestinal absorption of a poorly soluble drug [8]. To exploit the strategy, two steps are essential; generation and maintenance of supersaturation described the concept of "spring and parachute" approach to promote and maintain supersaturation of high energy amorphous forms of drugs in solution [9]. The high energy amorphous form of the drug (spring) can induce the generation of a supersaturated solution in the gastrointestinal lumen. However, supersaturated drug solutions

are thermodynamically unstable and have a tendency to return to equilibrium state by drug precipitation. To inhibit drug precipitation and gain benefit from the supersaturated state, the increased concentration has to be maintained for a time period sufficient for absorption. Many pharmaceutical excipients can be used as parachutes, such as cellulose derivatives (methylcellulose, hydroxypropyl methylcellulose [HPMC], and hydroxypropyl cellulose), vinyl polymers (polyvinyl acetate, polyvinylpyrrolidone [PVP], and PVP/vinyl acetate), surfactants, and β -cyclodextrin derivatives. High-energy or rapidly dissolving solid forms of drugs can be generated by altering morphology, particle size, and/or wettability. Solid dispersions, nanoparticles, coground mixtures; the use of inorganic matrices as a carrier, crystalline salt forms, and prodrugs of higher aqueous solubility are some techniques can be used for the formation of high energy amorphous form of drugs in solution [10].

Glibenclamide (GLB) is a sulfonylurea oral hypoglycemic agent belonging to BCS Class II. Its elimination half-life is approximately 2–5 h after oral administration, and it is 84±9% absorbed from GIT, but its bioavailability is low due to its poor solubility and extensive first-pass metabolism in liver [11,12].

The objective of this study was to improve the solubility of GLB using various carriers and incorporating the same into tablet dosage form.

MATERIALS AND METHODS

Materials

GLB was provided as a gift sample from USV Pharma, Mumbai (India). Syloid FP 244 EU and Syloid XDP 3050 were provided as a gift sample

from Grace Davison (Grace DMBH, and Co. KG, Germany) and were used as obtained. The other chemicals used for the study were of analytical grade.

Methods

Physicochemical characterization of GLB

Physicochemical characteristics of GLB were studied, namely, determination of melting point by recording a differential scanning calorimeter (DSC) thermogram, powder X-ray diffraction (PXRD) studies, pH-dependent solubility, flow properties, and determination of calibration curve (CC).

DSC analysis

The calorimetric analysis was carried out using LAB METTLER STAR SW DSC. 10 mg of sample was placed in a closed DSC aluminum pan and was heated at a constant rate of 10°C/min in the temperature range of 30–300°C in a dry nitrogen environment.

XRD analysis

The XRD pattern of API was measured with X'Pert PRO MPD X-ray diffractometer using the software X'Pert Data Collector. Radiations were generated from copper K-alpha electrode and filtered through nickel (Ni) filter with a wavelength of 1.5405 Å at a power of 45 KV and 40 mA were used to study X-ray diffraction patterns. The instrument was operated over the 2θ range of 10–90°.

Flow properties

Flow properties of GLB were calculated by determining the bulk density, tapped density, and angle of repose. Carr's index (CI) and Hausner's ratio were calculated.

- Bulk density (ρ_B)

The bulk density of the powder was determined as per the procedure described in IP 2010. It was calculated using the following formula:

Bulk density (ρ_B) (g/ml) = Weight of a sample in grams/ V_0 , where V_0 = Bulk volume.

- Tapped density (ρ_T)

The tapped density of the powder was determined as per the procedure described in IP 2010. Tapped density was calculated using the following formula:

Tapped density (ρ_T) (g/ml) = Weight of a sample in grams/ V_t , where V_t = Tapped volume.

- CI

Compressibility index measures the propensity of the powder to be compressed and also influences the flow properties since it is affected by the interparticle interactions. It is determined according to the procedure described in IP 2010. It is calculated from the following equation:

Compressibility index = (Tap density-Bulk density)/Tap density*100

- Hausner's ratio (H)

The Hausner's ratio is a number that is correlated to the flowability of a powder or granular material. The Hausner's ratio is calculated by the formula:

$H = \rho_B/\rho_T$, where, ρ_B = Bulk density, ρ_T = Tapped density.

- Angle of repose (θ)

The angle of repose is a characteristic related to interparticulate friction or resistance to movement between particles. The angle of repose has been defined as the maximum angle possible between the surface of a pile of powder and horizontal plane. It was determined using the fixed funnel method. A weighed amount of drug was poured through a funnel to form a cone. The angle of repose (The inverse tangent of the ratio of the height of the cone and radius of the base of the cone) was determined by measuring the height of the cone of the powder and radius of the base of the cone. It was calculated from the following formula.

$\tan \theta = h/r$, where, θ = Angle of repose, h = Height of the pile, r = Average radius of the powder cone.

Solubility study

Different buffers of pH 1.2, 4.5, 6.8, and 7.4 were prepared according to the procedure in USP. Excess amount of drug was added to 10 mL buffer in separate vials. These vials were then vortexed for 5 min and shaken for 24 h on an orbital shaker. The solutions were filtered and diluted appropriately. The samples were analyzed spectrophotometrically (Jascaow) for drug content at 300 nm.

CC

A CC for estimation of the drug was constructed by dissolving the drug in methanol and recording the ultraviolet (UV) absorbance of different concentration of drug solution in the range of 20–100 ppm at λ_{max} of 300 nm.

Formation of drug-carrier complex

The solid dispersion of GLB with PEG 6000

Solid dispersions of GLB were prepared using PEG 6000 by melt congealing method [13]. In this method, the drug was incorporated, into the molten carrier (70±5°C), and heated until a homogeneous melt was obtained and then cooled at room temperature. The resulting solid dispersions were stored for 24 h in desiccators at room temperature then pulverized and sieved.

Inclusion complex of GLB with β -cyclodextrin

Inclusion complex of GLB and β -cyclodextrin was formed by kneading method [14]. In this method, GLB was added to the slurry of β -cyclodextrins (amount of water taken was twice the weight of powder mixtures) and was kneaded in a mortar for 30 min. The pastes were dried at 45°C and sieved through #80.

Adsorption of GLB on mesoporous silica

GLB was loaded onto mesoporous silica by impregnation solvent evaporation technique using rotary flash evaporator [15]. A weighed amount of GLB was dissolved in dichloromethane. The solution was transferred in a round bottom flask (RBF). Mesoporous silica was then added to this solution followed by gentle shaking and sonication for 15 min. The RBF was then attached to rotary evaporator and the solvent was evaporated at 57°C under vacuum.

Different batches of solid dispersions, inclusion complex, and adsorption onto carriers are portrayed in Table 1.

Table 1: Drug-carrier complexes of GLB

Batches	A1	A2	A3	A4	A5	A6	A7	A8
Drug	GLB	GLB	GLB	GLB	GLB	GLB	GLB	GLB
Carrier	Syloid XDP 3050	Syloid XDP 3050	Syloid XDP 3050	Syloid FP 244	Syloid FP 244	PEG 6000	PEG 6000	β -cyclodextrin
Amount of drug (g)	0.5	0.5	0.5	0.5	0.5	0.5	0.5	0.5
Amount of carrier (g)	1	2	3	1	3	3	5	0.5
Drug:carrier ratio	1:2	1:4	1:6	1:2	1:6	1:6	1:10	1:1

GLB: Glibenclamide

Evaluation of drug-carrier complex

The drug-carrier complexes were assessed for flow properties to determine the enhancement of flow percent drug loading and enhancement of solubility and *in vitro* drug release.

Evaluation of flow properties

The drug-carrier complex was evaluated for flow properties, namely, bulk density, tapped density, CI, Hausner's ratio, and angle of repose. The procedure for determining flow properties is as described in the section of flow properties.

Determination of drug loading in drug-carrier complex

The total amount of drug-loaded in the carrier was quantified by UV spectrophotometry method. Drug loading in drug-carrier complex was evaluated by extracting the drug from the drug-carrier complex in methanol by vigorous shaking followed by centrifugation and appropriate dilution of the supernatant with methanol. These dilutions were analyzed using a UV-spectrophotometer at the λ_{max} of 300 nm.

Evaluation of drug release from the drug-carrier complex

A dissolution test was carried out in 900 ml of phosphate buffer pH 7.4 using the USP type II dissolution apparatus (Lab India DS 800) at $37 \pm 2^\circ\text{C}$ and 75 rpm for the duration of 1 h. Aliquots of 5 ml were withdrawn at 5, 10, 20, and 30 min and filtered, and then suitably diluted. UV absorbance measured at 227 nm. The concentration was estimated from the appropriate CC constructed in a pH 7.4 buffer solution.

Optimization of selected drug: Carrier complex

A 3^2 full factorial experimental designs were used, to optimize the amounts of the drug (X1) and carrier (X2). The different ratios were investigated to provide maximum drug dissolved in 30 min. The response variable studied was percent yield (Y1), percent drug loading (Y2), and percent drug dissolved (Y3) at 30 min. Table 2 provides an overview of the design of the study.

All experiments were performed in a randomized manner to eliminate any unknown possible sources of bias. Data obtained from all the formulations were analyzed using the Design Expert Software 9.0.4 and were used to generate the study design and 3D surface plot. The appropriate factorial model was generated for the response variable using the software. Several statistical parameters, including the coefficient of variation, regression coefficient (R^2), and adjusted regression coefficient (adjusted R^2) provided by Design-Expert software were compared, and the best fit was selected. In addition, analysis of variance (ANOVA) was used to identify significant effects of factors on response regression coefficients. The F test and P values were also calculated using the software. Table 3 details on the optimization batches of drug adsorption onto a mesoporous carrier (Syloid XDP 3050). The drug adsorbates were evaluated for drug loading and drug release from drug-adsorbate.

Determination of crystallinity of GLB

A selected batch of drug-adsorbate was characterized using PXRD and DSC to determine any change in the crystalline character of GLB.

DSC and PXRD were examined to study the polymorphic form (crystalline or amorphous) of pure GLB and GLB that is adsorbed onto Syloid XDP 3050.

DSC analysis was carried out using LAB METTLER STAR SW DSC instruments. 10 mg of a sample was placed in a closed DSC aluminum pan and was heated at a constant rate of $10^\circ\text{C}/\text{min}$ in the temperature range of $30\text{--}300^\circ\text{C}$ under a dry nitrogen environment. The XRD pattern of GLB and GLB:Syloid XDP 3050 was measured with a view to understanding the polymorphic form of GLB in drug adsorbate and its pure form. This was measured with X'Pert PRO MPD X-ray diffractometer using the software X'Pert data collector. The instrument was operated over the 2θ range of $10\text{--}90^\circ$.

Determination of surface characteristics of drug adsorbate by scanning electron microscopy (SEM)

The morphology and particle size of the pure GLB and GLB adsorbed Syloid XDP 3050 were examined using SEM. The images of the above samples were viewed under Jeol5400 SEM (Jeol, Japan) after sputter coating with gold in Fine Coat Ion JFC 1100 sputter (Jeol, Japan) for 5–6 min.

Formulation development of tablets using the adsorbed drug

Amount of drug-adsorbate equivalent to 5 mg GLB was accurately weighed. Tablet blends were prepared using HPMC E-5 as precipitation inhibitor, sodium starch glycolate, and croscarmellose sodium as superdisintegrant, PVP K30 as dry binder, and microcrystalline cellulose PH 102 as diluents, and magnesium stearate as a lubricant. Required amounts of all excipients other than the lubricants were separately sifted through no. #60 accurately weighed and mixed with the drug-adsorbate. This was followed by the addition of lubricants. The mixture was blended for about 3 min. The blends were evaluated for flow properties. Lubricated blend was compressed using 6 mm biconvex punch. Formulations are described in Table 4.

Evaluation of tablets

Formulated tablets were evaluated for different parameters such as tablet dimensions, weight variation, hardness, friability, and disintegration time, and analytical parameters such as dissolution profile and assay were evaluated. Dissolution of the tablet was carried out in USP apparatus II (Paddle) using 900 ml pH 7.4 phosphate buffer as dissolution medium at 37°C at 10, 20, 30, 45, and 60 min. *In vitro* release profile of formulated tablet was compared with the marketed tablet.

RESULTS AND DISCUSSION

Characterization of GLB

DSC and melting point

The crystalline form of the drug along with its melting point was evaluated by DSC analysis which showed a sharp endothermic peak in the DSC curve indicating the presence of the drug in crystalline form

Table 2: Coding of the actual values for 3^2 full factorial designs

Factor (Independent variable)	Levels		
	High (+1)	Medium (0)	Low (-1)
Drug (X1)	33.33	20	14.28
Carrier (X2)	85.72	80	66.66

Dependent variables – % yield (Y1), % drug loading (Y2) and % drug dissolved (Y3) at 30 min

Table 3: Composition of batches for optimization of the amount of carrier and amount of drug

Independent variables	Optimization trials								
	F1	F2	F3	F4	F5	F6	F7	F8	F9
Amount of GLB	+1	+1	+1	0	0	0	-1	-1	-1
Amount of Syloid XDP 3050	+1	0	-1	+1	0	-1	+1	0	-1

Table 4: Formulation and development of glibenclamide immediate release tablet. (*Quantities in mg)

Ingredient	B1	B2
Drug-adsorbate (equivalent to 5 mg drug)	35.31	35.31
HPMC E-5	-	30
PVP-K 30	3	3
Sodium starch glycolate	2	2
Croscarmellose sodium	2	2
Microcrystalline cellulose PH 102	57.49	27.49
Talc	0.2	0.2
Total (mg)	100	100

at its melting point 174.27°C. The endothermic peak of GLB by DSC analysis is represented in Fig. 1. Fig. 1 shows that the procured drug complies with the reported results.

PXRD

GLB was further analyzed by PXRD to confirm its crystallinity. The diffraction pattern of the crystalline drug GLB is represented in Fig. 2. The appearance of sharp peaks confirmed the crystalline nature of the drug.

Flow properties

Determination of angle of repose, CI, and Hausner's ratio showed that GLB has very poor flow. The poor flow can be attributed to the fine particle size of the drug. The fine size results in the development of surface charge and adhesive forces that hinder the free-flowing properties of the drug. The results are depicted in Table 5.

Solubility study

The solubility of GLB was estimated at pH 1.2, 4.5, 6.8, and 7.4 buffers and water by determination of saturation solubility. Being a weakly acidic drug, GLB showed the highest solubility at basic pH (about 0.036 mg/ml). Table 6 describes the solubility of GLB in different media.

CC

CC of GLB was constructed in methanol by recording the absorbance's of 10, 20, 40, 60, 80, and 100 µg/ml and plotting these against the corresponding absorbance values. The regression coefficient value (R²) was calculated. The graph was found to be linear with a R² value of 0.999 and the straight line equation was found to be $y=0.006x+0.016$. The absorbance versus concentration CC of GLB in methanol is shown in Fig. 3.

Evaluation of drug-carrier complex

Different methods were employed for the formation of the drug-carrier complex. The drug-carrier complex was evaluated for flow properties and drug load content and *in vitro* drug release from drug-carrier complex.

Evaluation of flow properties and drug loading

The drug-carrier complex was evaluated for flow properties, namely, bulk density, tapped density, CI, Hausner's ratio, and angle of repose as per procedure mentioned in the section of evaluation of flow properties. The results for the flow parameters and drug load content of adsorbed drug are as follows in Table 7. Batch A1, A2, A3, A6, and A8 of the adsorbed drug had excellent flow properties with excellent to fair compressibility index. Batch A4 and A5 showed good flow properties with fair to passable compressibility index. Drug loading in drug-carrier complex was evaluated by the procedure mentioned above. Batch A3 and A6 showed a

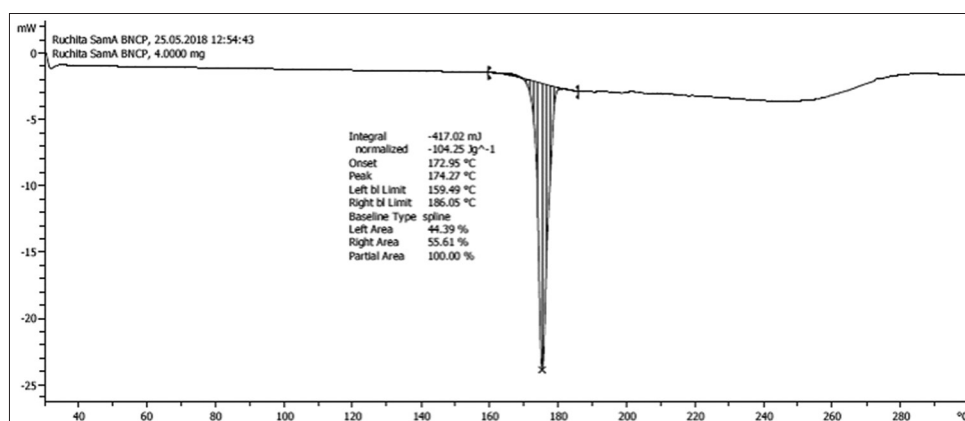


Fig. 1: Differential scanning calorimeter spectrum of glibenclamide showing a sharp endothermic peak

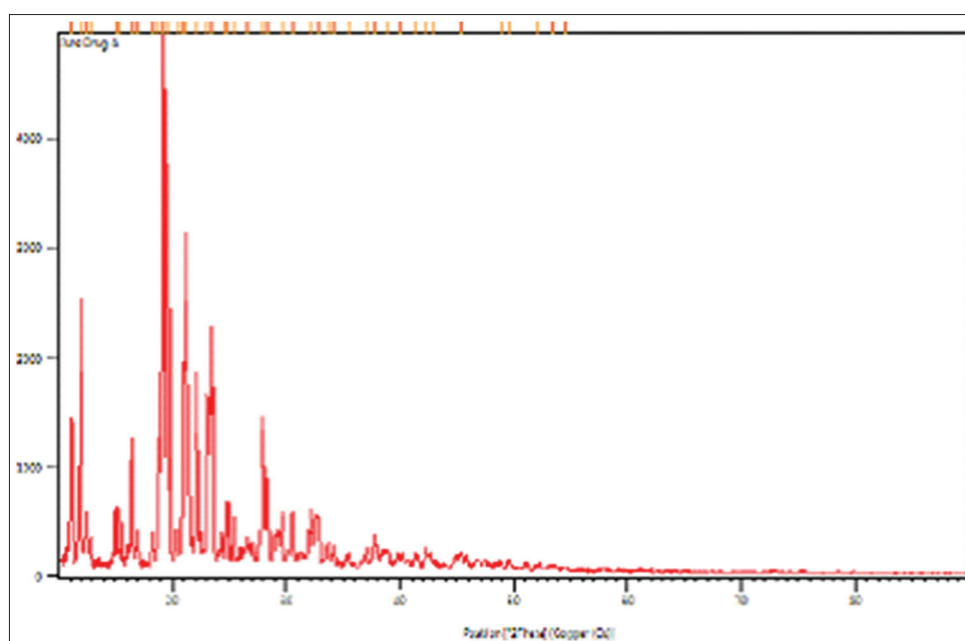


Fig. 2: Powder X-ray diffraction pattern of glibenclamide

Table 5: Flow properties of GLB

Flow properties	Observations	Inference	Reference range
Bulk density (g/ml)	0.2	-	-
Tapped density (g/ml)	0.28	-	-
Carr's index (%)	28.57	Poor flow	28-35
Hausner's ratio	1.4	Poor flow	1.35-1.45
Angle of repose (°)	33.1°	Good	31-35°

Table 6: Solubility results of GLB in various media

Medium	Solubility (mg/ml)
Water	0
pH 1.2 buffer	0.030
pH 4.5 buffer	0
pH 6.8 buffer	0
pH 7.4 buffer	0.036

GLB: Glibenclamide

higher percent drug loading than other batches. Batch A3 had GLB:Syloid XDP 3050 (1:6). The higher concentration of carrier resulted in better entrapment in the mesoporous structure. In A4 and A5, GLB: Syloid FP244 was used in 1:2 and 1:6 ratio. The percent drug loading was comparable to XDP 3050. Percent drug loading in A4 was 89.57% and A5 was 93.53%. In both A6 and A7, PEG 6000 was used as carrier and percent drug loading was 98.94 and 87.32, respectively. The higher drug loading is attributed to high carrier concentration in these batches.

Evaluation of drug release from the drug-carrier complex

Dissolution studies of all drug-carrier complexes were performed in USP apparatus II (paddle type) using phosphate buffer pH 7.4 as the dissolution medium. Initially, it was observed that the drug desorption was faster from Syloid XDP 3050 and Syloid FP 244 to generate a supersaturated drug solution. However, supersaturated solutions are thermodynamically unstable and have a tendency to return to equilibrium state by drug precipitation. Therefore, the solubility of GLB was rapidly decreased within 5 min. Hence, this problem was overcome using HPMC E-5 as a stabilizer or precipitation inhibitor. HPMC E-5 was physically mixed with drug-carrier complex, and drug release was observed. The drug release from Syloid XDP 3050 and Syloid FP 244 was almost 80% and 37%, respectively, in just 30 min which indicates that the drug solubility has been improved to a great extent. Drugs desorption from PEG 6000 and β -cyclodextrin was found to be less. Plain drug solubility was found to be approximately 2% at the end of 1 h. Fig. 4 depicts a graphical representation of the dissolution profile of an adsorbed drug. Hence, from the results, Syloid XDP 3050 was selected as a carrier. Since it gave improved flow properties as well as increases the solubility.

Batch	Drug: Carrier
A1	GLB: Syloid XDP 3050 (1:2)
A2	GLB: Syloid XDP 3050 (1:4)
A3	GLB: Syloid XDP 3050 (1:6)
A4	GLB: Syloid XDP 3050 (1:2)
A5	GLB: Syloid XDP 3050 (1:6)
A6	GLB: PEG 6000 (1:6)
A7	GLB: PEG 6000 (1:10)
A8	GLB: β -cyclodextrin (1:1)

Optimization of drug adsorption using SYLOID XDP 3050

Drug adsorption was optimized by a 3² factorial design. An overview of the experimental trials and the responses obtained is presented in Table 8. The obtained results of drug dissolved at the end of 30 min were fitted in the Design Expert Software 9.0.4 and it was statistically analyzed for the response variable using the same. A total of nine formulations was proposed by 3² factorial design for the two independent variables (i.e., Drug X1 and Carrier X2) varied at three different levels [high (+1), medium (0), and low (-1)].

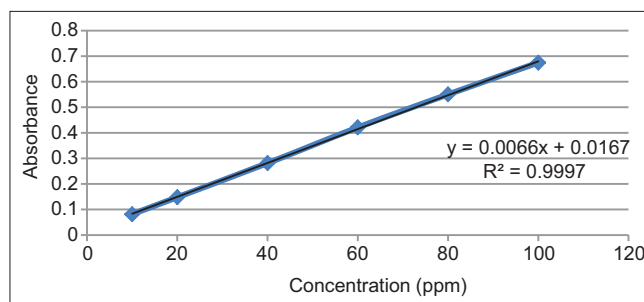
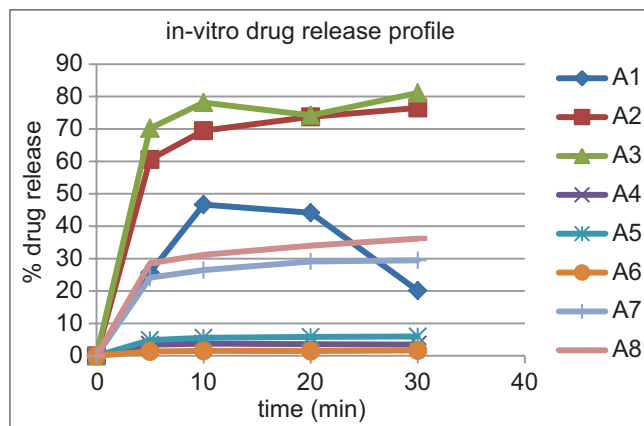
Fig. 3: Ultraviolet calibration curve of glibenclamide in methanol at λ_{max} 300 nm

Fig. 4: Graphical representation of dissolution profile of an adsorbed drug

Effect of independent variables (amount of drug and amount of carrier) on dependent variable percent yield

Analysis of the statistical parameters showed that the selected model is significant. The results of the ANOVA for the selected model are shown in Table 9 that indicated that the selected model was significant for the response variable (percent yield) studied. The model F-value obtained was 7.47. In this model, A (drug), B (carrier), and AB (interaction of A and B) are significant model terms. The results of the statistical parameters for the model selected are presented in Table 10.

The optimized model equation for the response variable (Y1) is given as follows:

$$\% \text{ yield at 30 min (Y1)} = +96.63 + 1.33 * A(\text{drug}) + 1.83 * B(\text{carrier}) - 1.75 * A(\text{drug}) * B(\text{carrier}) \quad (1)$$

It is observed from the Equation no. 1 that the coefficient b1 and b2 are positive, and coefficient b1b2 is negative. It implies that interaction between drug and carrier has an antagonistic effect on the response variable – percent yield.

The model F-value of 7.47 implies that the model is significant. There is only a 1.38% chance that an F-value this large could occur due to errors. $p < 0.0500$ indicates that model terms are significant. Precision measures the signal to noise ratio. A ratio > 4 is desirable. The obtained ratio of 8.569 indicates an adequate signal (model is significant). This model can be used to navigate the design space. Design expert Software generated interaction plot and 3D surface response plot that are represented in Figs. 5 and 6. The interaction plot shows that the high level of the carrier has a positive effect (maximum percent yield) on the response variable at varied levels of drug, whereas the low level of the carrier has a negative effect (minimum percent yield) with the low level of the drug.

Table 7: Flow properties and percent drug loading of batches

Parameters	A1	A2	A3	A4	A5	A6	A7	A8
Bulk density (g/ml)	0.33	0.312	0.303	0.166	0.130	0.52	0.48	0.48
Tapped density (g/ml)	0.416	0.370	0.333	0.217	0.178	0.59	0.56	0.65
Carr's index (%)	20	15.62	9.09	23.33	26.31	12	14.81	25.80
Hausner ratio	1.24	1.18	1.09	1.30	1.35	1.13	1.16	1.34
Angle of repose (°)	26.8	23.5	22.2	32.7	30.3	23	23.3	42.82
Flow rate (s)	0.99	0.94	0.90	1.2	0.99	0.95	0.99	3.67
Drug loading (%)	96.57	93.25	99	89.57	93.53	98.94	87.32	90.64

Table 8: Summary of the 3² factorial designs

Batch	Run	Factor 1 A: Drug Mg	Factor 2 B: Carrier Mg	Response 1 % yield %	Response 2 % drug loading %	Response 3 % drug release %
F1	1	+1	+1	99	99.32	67
F2	2	+1	0	96	99.18	64.12
F3	3	+1	-1	98	96.57	20.12
F4	4	0	+1	98	98.41	72.25
F5	5	0	0	97	93.25	76.5
F6	6	0	-1	96	89.55	62.92
F7	7	-1	+1	98	99	81.31
F8	8	-1	0	97	93.25	63.65
F9	9	-1	-1	90	98.29	66.06

Table 9: ANOVA table for the dependent variable (% yield) from 3² factorial designs

Source	Sum of squares	Df	Mean square	F value	p value Prob.>F	Significant
Model	43.08	3	14.36	7.47	<0.05	Significant
A-drug	10.67	1	10.67	5.55	<0.05	
B-carrier	20.17	1	20.17	10.49	<0.05	
AB	12.25	1	12.25	6.37	<0.05	
Pure error	0.0000	2	0.0000			
Cor total	56.55	10				

Table 10: Statistical data for selected factorial model

Parameter	Value
Regression coefficient (R ²)	0.7619
Adjusted Regression coefficient (adjusted R ²)	0.6599
Predicted R ²	0.0538
Coefficient of variation (%)	1.44
Adeq precision	8.569

Table 11: ANOVA table for the dependent variable (percent drug loading) from 3² factorial designs

Source	Sum of squares	df	Mean square	F value	p value Prob.>F	Significant
Model	111.56	7	15.94	41.54	<0.005	Significant
A-drug	17.58	1	17.58	45.83	<0.005	
B-carrier	39.25	1	39.25	102.30	<0.005	
AB	1.04	1	1.04	2.71	<0.005	
A ²	34.22	1	34.22	89.20	<0.005	
B ²	5.26	1	5.26	13.70	<0.005	
A ² B	16.95	1	16.95	44.17	<0.005	
AB ²	14.65	1	14.65	38.19	<0.005	
Pure error	0.0000	2	0.0000			
Cor total	112.71	10				

Effect of independent variables (amount of drug and amount of carrier) on dependent variable percent drug loading and percent drug release at 30 min

The analysis of the statistical parameters also showed that the selected model is significant. The results of the ANOVA for both the response

Table 12: ANOVA table for the dependent variable (percent drug release) from 3² factorial designs

Source	Sum of squares	Df	Mean square	F value	p value Prob.>F	Significant
Model	2720.23	7	388.60	138.36	0.0009	Significant
A-drug	0.1104	1	0.1104	0.0393	0.8555	
B-carrier	43.52	1	43.52	15.50	0.0292	
AB	250.11	1	250.11	89.05	0.0025	
A ²	289.64	1	289.64	103.13	0.0020	
B ²	123.87	1	123.87	44.10	0.0070	
A ² B	157.47	1	157.47	56.07	0.0049	
AB ²	312.02	1	312.02	111.09	0.0018	
Pure error	0.0000	2	0.0000			
Cor total	2728.65	10				

Table 13: Statistical data for selected factorial model

Parameter	Percent drug loading	Percent drug release at 30 min
Regression coefficient (R ²)	0.9898	0.9969
Adjusted Regression coefficient (adjusted R ²)	0.9660	0.9897
Predicted R ²	0.2975	0.6077
Coefficient of variation	0.6469	2.54
Adeq precision	18.2302	42.81

variables (i.e., percent drug loading and percent drug release at 30 min) for the selected model are shown in Tables 11 and 12. Responses, namely, percent drug loading and percent drug release at 30 min were studied. The model F-value obtained was 41.54, 138.36 for the response variables percent drug loading and percent drug release, respectively, which implied that the model is significant. In this case, A, B, A², B², A²B, and AB² are significant model terms for the response variable percent drug loading and B², AB, A², B², A²B, and AB² are significant model terms for the response variable percent drug release at 30 min. The results of the statistical parameters for the selected model are presented in Table 13. The optimized equation for the model for the response variable (Y1) is given as follows.

$$\begin{aligned} \% \text{ Drug loading (Y2)} = & +92.97+2.97*A(\text{drug})+4.43*B(\text{carrier}) \\ & +0.5100*A(\text{drug})B(\text{carrier})+3.68*A^2(\text{drug})+1.44*B^2(\text{carrier}) \\ & -3.56*A^2(\text{drug})B(\text{carrier})-3.31*A(\text{drug})B^2(\text{carrier}) \end{aligned} \quad (2)$$

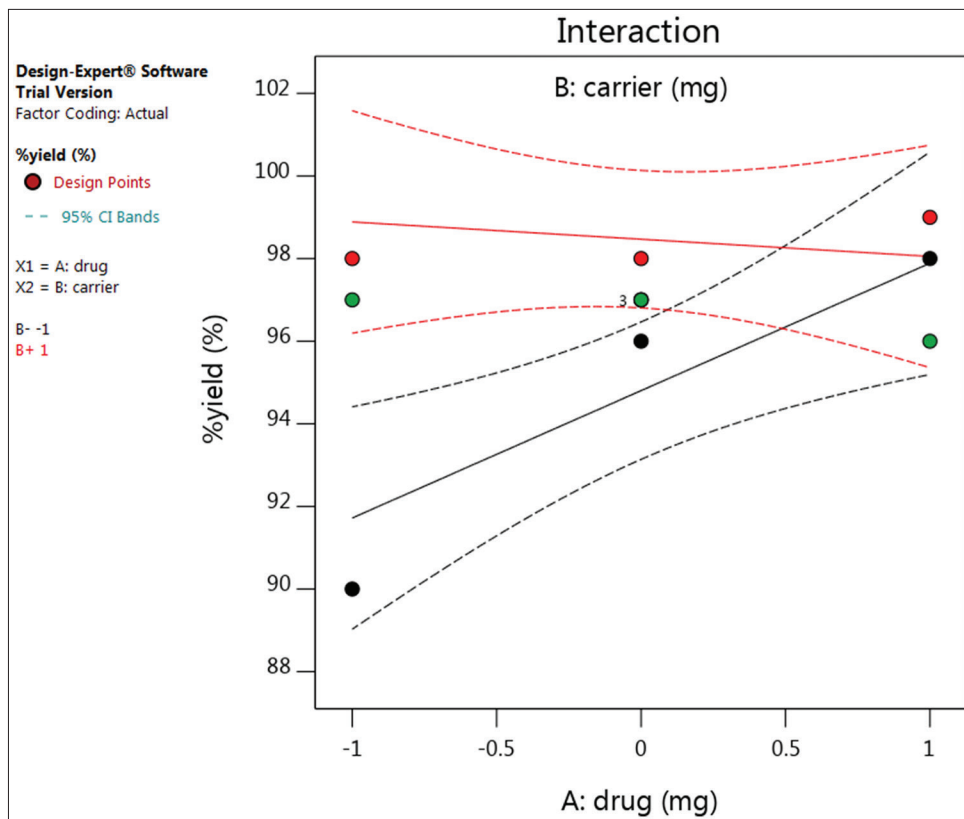


Fig. 5: Diagrammatic representation of the interaction of carrier and drug on percent yield

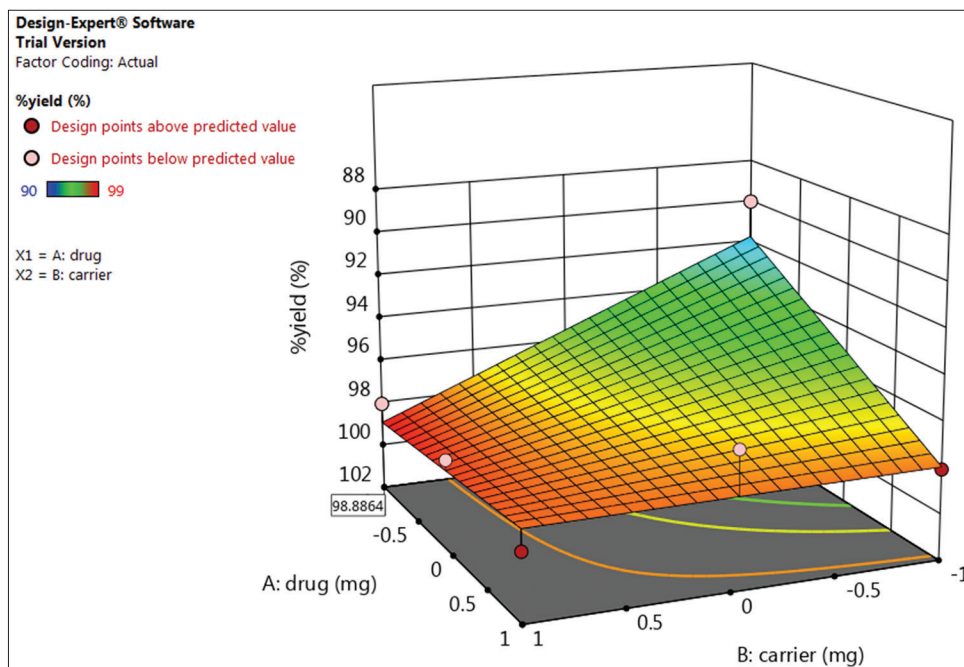


Fig. 6: 3D surface response plot of percentage yield

$$\% \text{ Drug release at 30 min (Y3)} = +75.73 + 0.2350 \cdot A(\text{drug}) + 4.67 \cdot B(\text{carrier}) + 7.91 \cdot A(\text{drug})B(\text{carrier}) - 10.69 \cdot A^2(\text{drug}) - 6.99 \cdot B^2(\text{carrier}) + 10.87 \cdot A^2(\text{drug})B(\text{carrier}) - 15.30 \cdot A(\text{drug})B^2(\text{carrier}) \quad (3)$$

It is observed from the Equation no. 2 that the coefficient B1, B2, B1b2, B1², and B2² are positive and coefficient B1²B2 and B1B2² are negative. It implies that interaction between drug and carrier. Equation 3 signifies

that the coefficient B1, B2, B1B2, and B1²B2 are positive and coefficient B1², B2², and B1B2² are negative. A negative sign indicates the interaction between both parameters. An interaction plot and 3D surface response plot generated by Design Expert Software are represented in Figs. 7-10 for percent drug loading and percent drug release at 30 min, respectively. In case of percent drug loading, interaction plot shows that the high level of the carrier has a positive effect on the response variable at varied levels of the drug whereas the low level has a strong negative

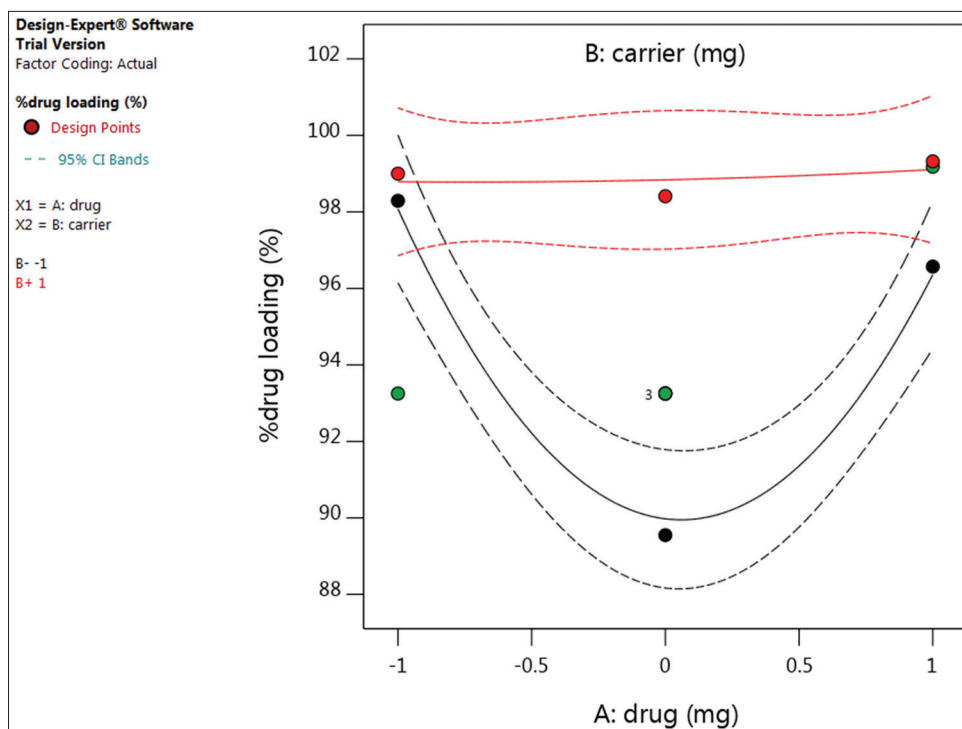


Fig. 7: Diagrammatic representation of the interaction of carrier and drug on percent drug loading

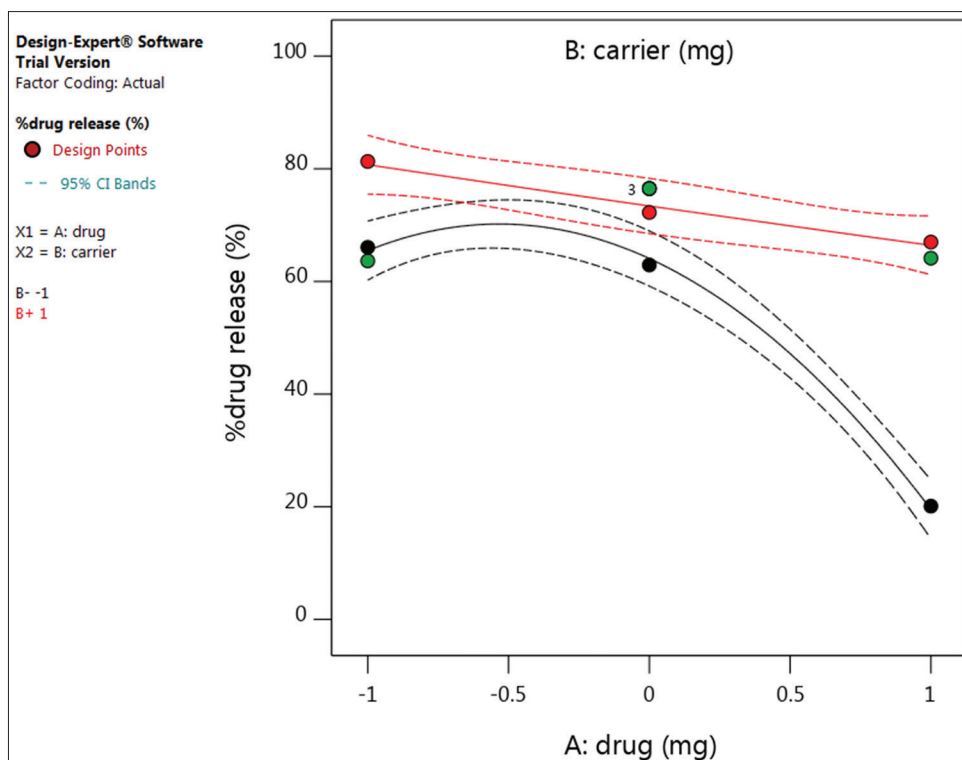


Fig. 8: Diagrammatic representation of the interaction of carrier and drug on percent drug release at 30 min

effect with the increased amounts of the drug. In case of percent drug release at 30 min, interaction plot shows that the high level of the carrier has a positive effect on the response variable at the low level of the drug whereas the low level of the carrier has a strong negative effect on the response variable at a high level of the drug.

The 3D surface plot shows the responses in a 3D view. In the case of percent drug loading, it was observed that the downward trend of wire mesh was at

a high level of drug and low level of carrier, upward trend of wire mesh was at high of carrier and low of drug and the other two responses (i.e., High of drug and high of carrier and low of drug and low of carrier) also positions toward upward. It is predicted that the dependent variable is directly proportional to the amount of carrier. Whereas in case of percent drug release at 30 min, it was observed that the downward trend of wire mesh was at a low level of the carrier and high level of the drug, and the upward trend of wire mesh was at a high level of the carrier and low level of the drug.

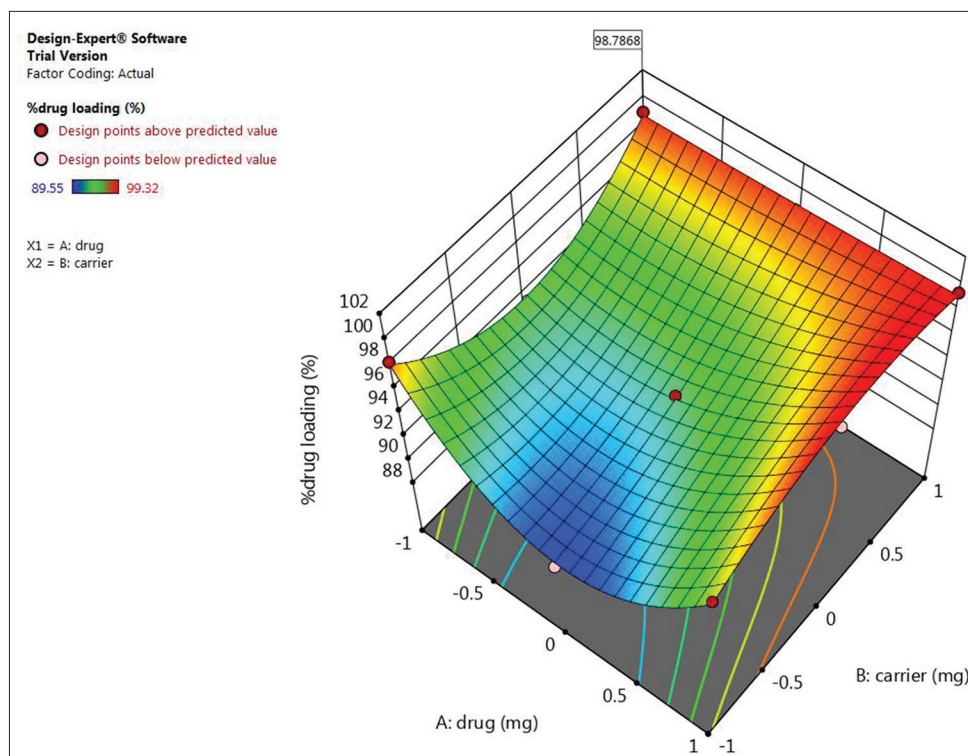


Fig. 9: 3D surface response plot of percent drug loading

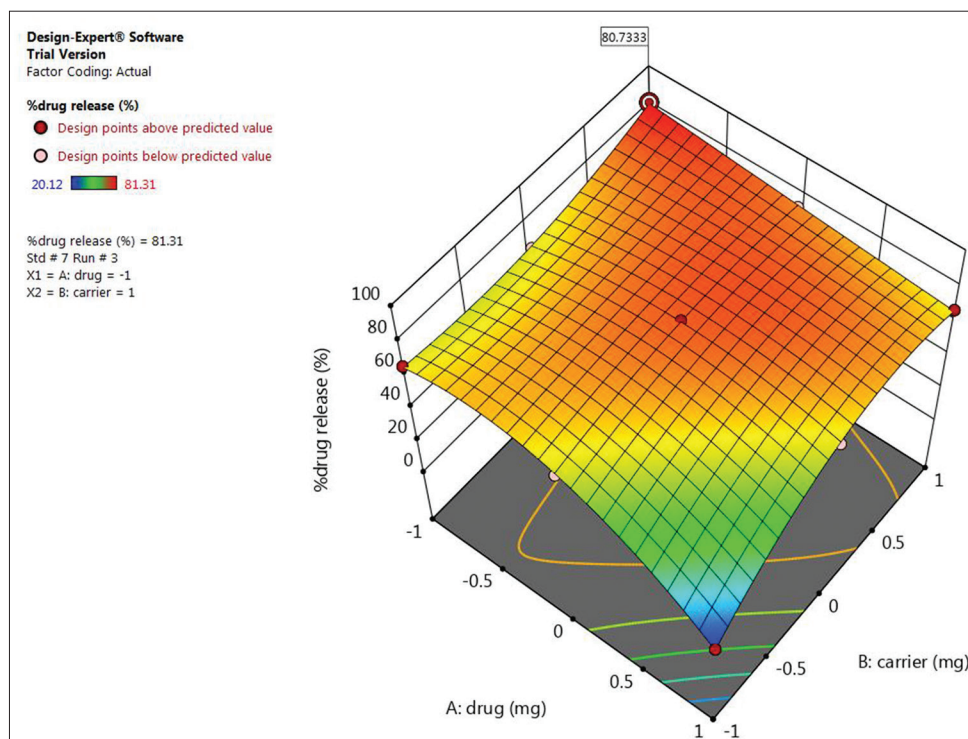


Fig. 10: 3D surface response plot of percent drug release

To optimize all the responses with different targets, a multi-criteria decision approach, a numerical optimization technique by the desirability function (Fig. 11), and a graphical optimization technique by the overlay plot (Fig. 12) were used. The optimized formulation was obtained by applying constraints on dependent variable responses (percent yield, percent drug loading, and percent drug release at 30 min) and independent variables (drug and

carrier). The recommended concentrations of the drug and carrier were calculated by the Design-Expert software from the overlay plot and the desirability plot which has the highest desirability near to 1.0.

The study design after optimization showed 100 solutions from which one solution giving maximum drug release with good drug loading and

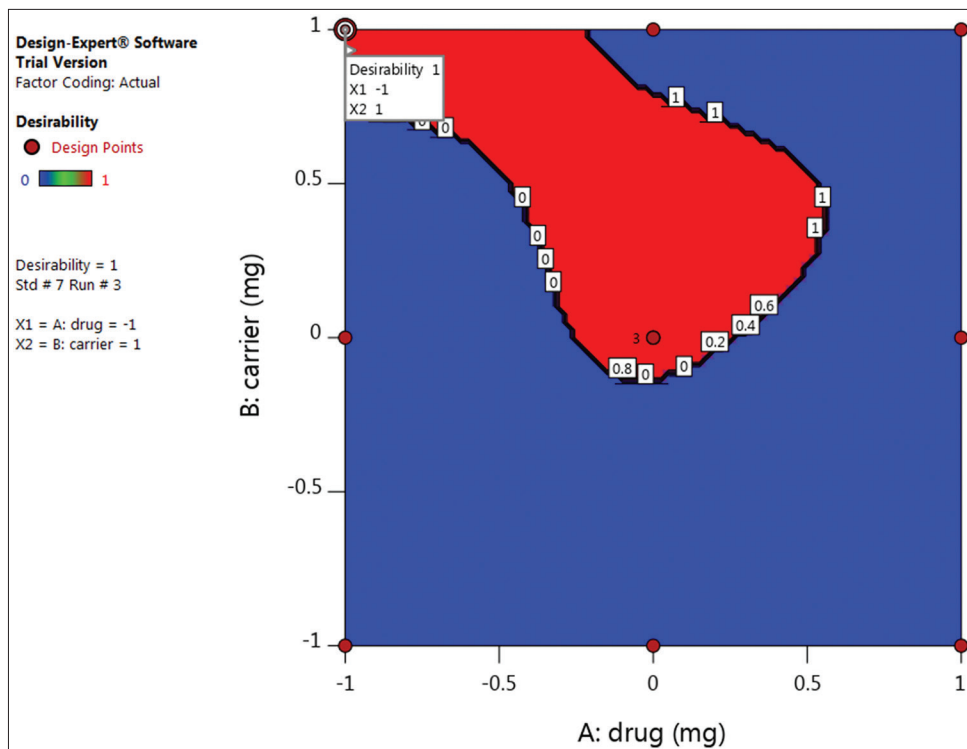


Fig. 11: Desirability plot for the optimization of drug-carrier concentration

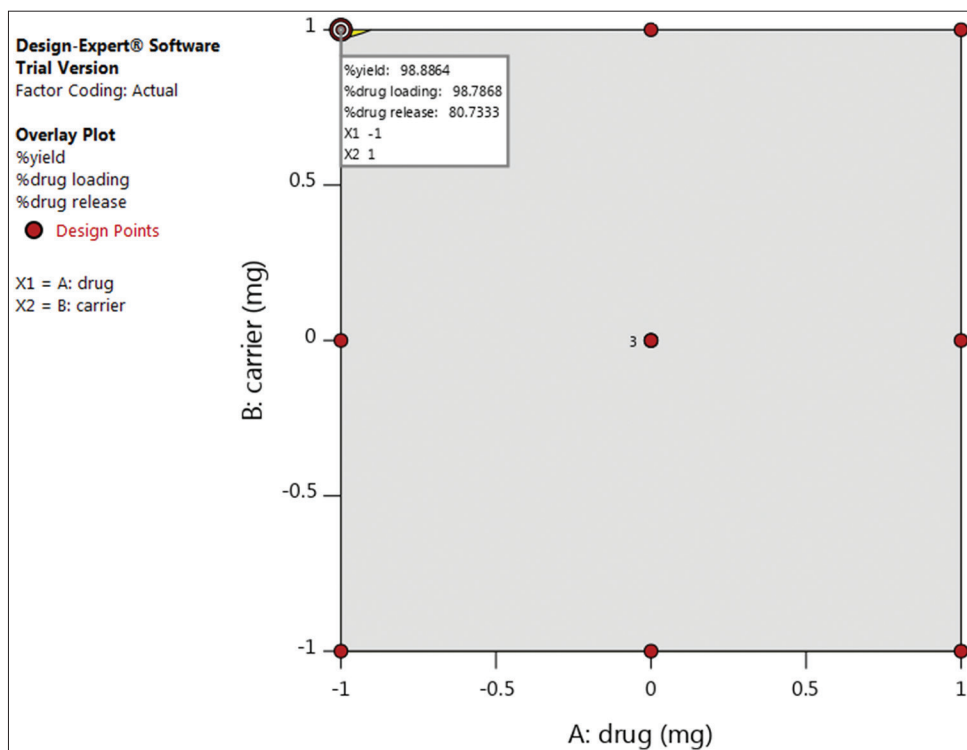


Fig. 12: Overlay plot of the constraints applied to the study design

percent yield was selected and studied validation of the model. The batch F7 showed optimum results as predicted.

Evaluation of batches for optimization of the amount of carrier

The batches of factorial design study were evaluated for drug loading and drug release from adsorbate. The results for the drug loading and drug release from the carrier are given in Table 14.

Fig. 13 shows that the drug release is more from batch F7 (81.31%) in 30 min followed by batch F5 (76.5%) and F4 (72.25%). The drug release from batch F3 is less (20.12%). This implies that more the amount of carrier taken for adsorption more the drug release in lesser time. Batch F3 shows slow release because of loading high amount of drug on less amount of carrier.

Batch	GLB	Syloid XDP 3050
F1	+1	+1
F2	+1	0
F3	+1	-1
F4	0	+1
F5	0	0
F6	0	-1
F7	-1	+1
F8	-1	0
F9	-1	-1

Characterization of the optimized batch

Characterization of the optimized batch by X-ray diffraction

The PXRD pattern of an optimized batch of GLB loaded Syloid XDP 3050 is represented in Fig. 14. The XRD pattern did not show any diffraction

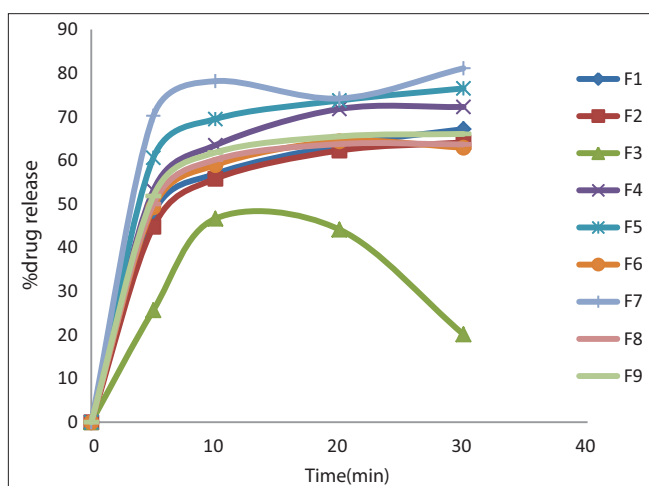


Fig. 13: Drug release profile of the adsorbate of the factorial batches

peaks that are characteristic of the crystalline form of the drug. It implies that the drug changed its polymorphic form and converted to the amorphous form.

Characterization of the optimized batch of an adsorbed drug by SEM

Fig. 15 depicts the morphology of GLB-loaded Syloid XDP3050. Drug adsorption can be seen on the surface of Syloid. The irregular shaped the crystalline structure of GLB is lost, indicating a change in its polymorphic form.

Characterization of the optimized batch of an adsorbed drug by DSC

DSC thermogram of batch F7 showed in Fig. 16 further confirmed the loss of crystallinity of GLB after loading onto Syloid XDP 3050. As compared with pure GLB, changes in melting point, peak onset ultimately proved that GLB was loaded on and/or into Syloid XDP 3050.

Evaluation of formulation development of tablets using the adsorbed drug

The drug-mesoporous silica adsorbate exhibited excellent flow properties and compressibility. Thus, in this work, the direct compression method was adopted to prepare tablets. All the excipients used were of direct compression grade. Superdisintegrants (namely, sodium starch glycolate and croscarmellose sodium) were used in tablet formulation as they have the ability to rapidly disintegrate tablet thereby facilitating an immediate drug release. HPMC E 5 was used as a stabilizer in the formulation to inhibit the precipitation of drug in the dissolution medium.

Evaluation of pre-compression parameters of the blend

Blends B1 and B2 were evaluated for flow properties. Results of the flow characteristics are shown in Table 15. It was observed that both batches B1 and B2 showed good flow, as depicted in Table 15. From the results, it can be thus concluded that all the blends possess suitable compressibility and can be tableted using direct compression technique.

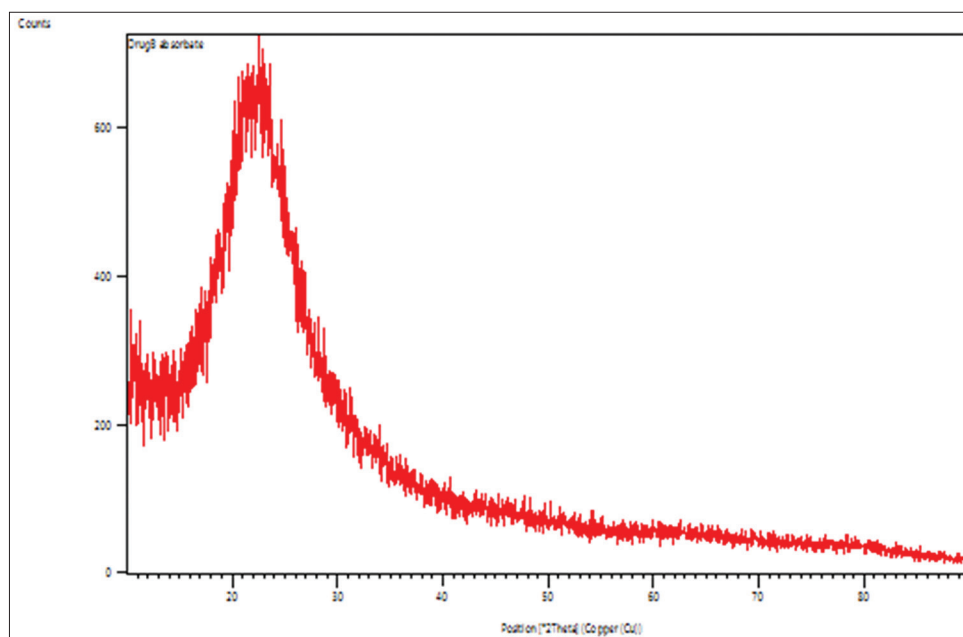


Fig. 14: X-ray diffraction pattern of the optimized batch of drug adsorbate

Table 14: Results for factorial batches

Parameters	F1	F2	F3	F4	F5	F6	F7	F8	F9
Percent drug loading	99.32	99.18	96.57	98.41	93.25	89.55	99	93.25	98.29
Percent drug release at 30 min	67.17	64.12	20.12	72.25	76.50	62.92	81.31	63.65	66.06

Evaluation of post-compression parameters of the tablets

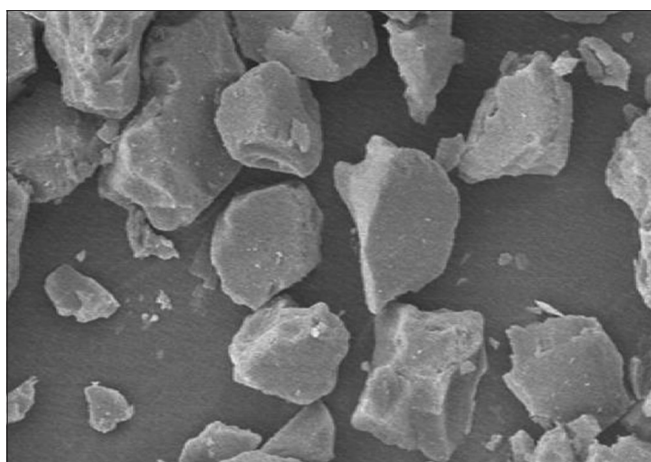
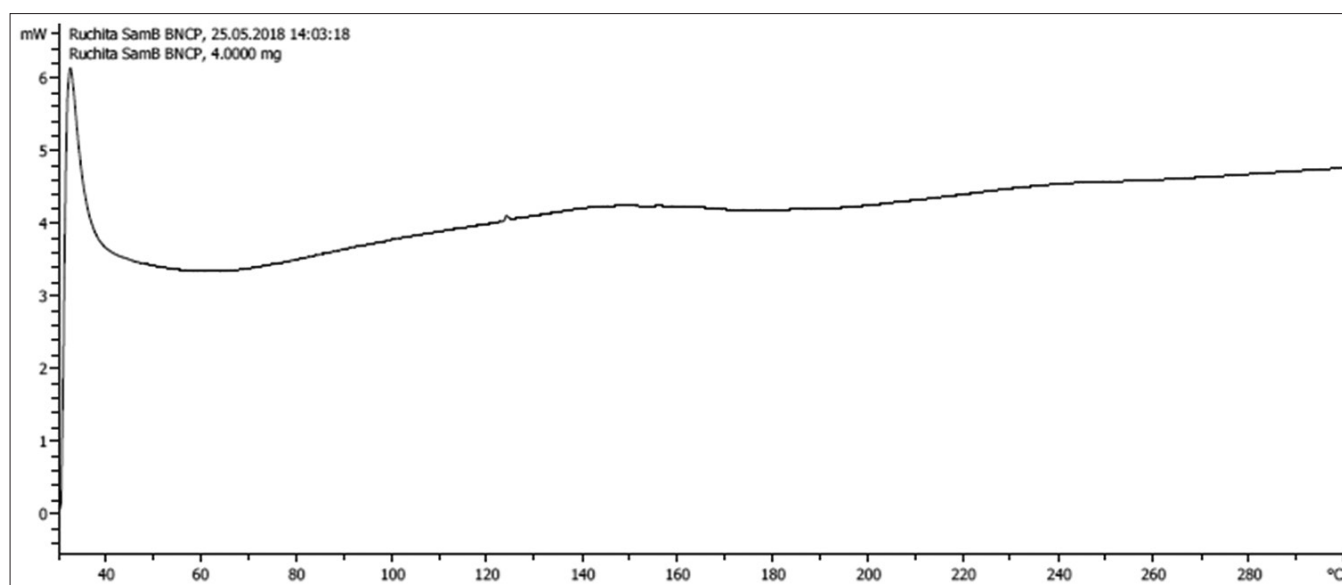
The pre-compression blends were compressed to form tablets using a mini-press 12 station tablet compression machine using 6 mm punch

Table 15: Pre-compression evaluation of batches B1 and B2

Parameters	B1	B2
Bulk density (g/ml)	0.357	0.344
Tapped density (g/ml)	0.434	0.434
Carr's index (%)	17.85	20.68
Hausner's ratio	1.21	1.26
Angle of repose (°)	21.53	21.41
Inference	Good flow	Good flow

Table 16: Post-compression evaluation of batch B1 and B2

Physical parameters	B1	B2
Appearance	Circular, biconvex, white tablets	
Average weight	98	101
Average thickness	3.42	3.46
Average hardness	4-5	4-5
Disintegration	7 min 45 s	9 min 24 s
Weight variation	Complies	Complies
Friability (%)	0.46	0.23
Assay (%)	98.37±2.31	97.21±1.28

**Fig. 15: Scanning electron microscopy of drug adsorbate****Fig. 16: Differential scanning calorimeter spectrum of batch A7**

of biconcave, circular shape. The compressed tablets were evaluated for physical parameters, assay, and *in vitro* drug release profile studies.

Physical parameters

Results of the physical evaluation of the post-compression parameters are shown in Table 16. The results show that the physical parameters of all the trial batches were found to be within limits.

Assay

Results of the content uniformity of the trial batches are represented in Table 16. The results are expressed in the form of mean±SD. All the batches showed above 90% drug content.

***In vitro* dissolution studies of batches B1 and B2**

In vitro drug release study was performed on the tablets as per the procedure mentioned in the section of evaluation of drug release from the drug-carrier complex. Drug release profiles from the batches B1 to B2 are illustrated in Fig. 17. Drug release studies of tablets from batches B1 to B2 revealed that batches B2 containing HPMC E5 showed maximum drug release at 30 min. Batch B1 without HPMC E5 showed least drug release.

Comparison of *in vitro* drug release profile of selected tablet and marketed tablet

In vitro drug release study was performed on the tablets as per the procedure mentioned in the section of evaluation of drug release from the drug-carrier complex. Fig. 18 showed a graphical representation of drug release profiles of both tablets.

The graphical representation showed that within 30 min, the 86% drug released from formulated tablet, whereas marketed tablet showed only 34.93% drug release after 30 min.

CONCLUSION

The solubility of GLB was enhanced by loading onto SYLOID® XDP 3050 matrix. Furthermore, the dissolution profile of GLB-loaded SYLOID® XDP 3050-containing tablets was also improved as compared with conventional and commercially available GLB tablets. This study indicates that non-ordered mesoporous SYLOID® XDP 3050 is a promising carrier, which enhances the oral bioavailability of poorly water-soluble drugs. Preparing a tablet dosage form containing drug-loaded silica may represent a new approach for the development of better absorbed oral formulations for poorly soluble drugs.

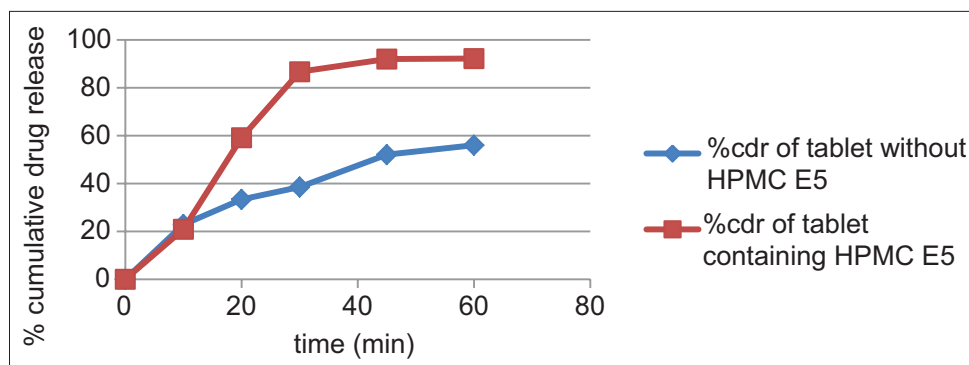


Fig. 17: *In vitro* drug release studies on tablet batches B1 and B2

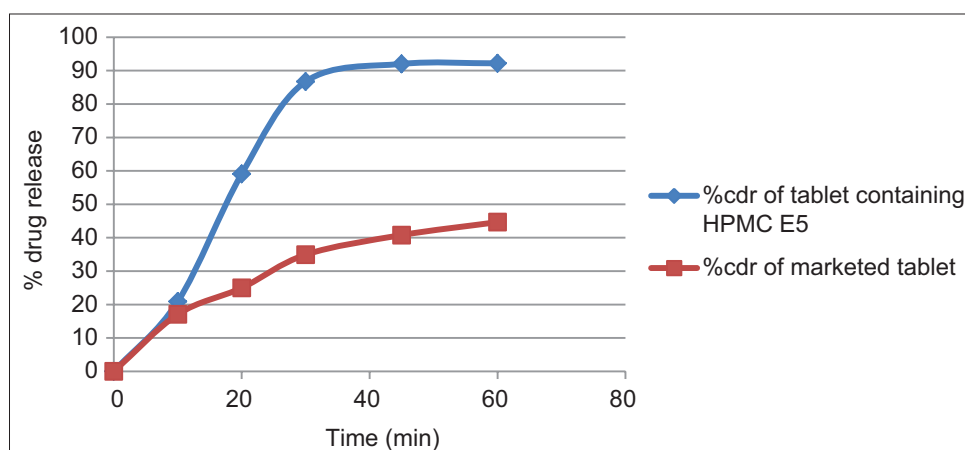


Fig. 18: Dissolution profiles of formulated tablet and marketed table

Conclusively, the current study attained the successful design, preparation, and evaluation of drug-loaded SYLOID® XDP 3050-containing GLB tablets.

AUTHORS' CONTRIBUTION

Dr. Swati Mittal designed the experimental study and performed the statistical analysis. Akshay Sonawane and Mangesh Khune carried out the experimental part and participated in the sequencing alignment and drafted the manuscript.

CONFLICTS OF INTEREST

The authors declare that they have no conflicts of interest.

REFERENCES

- Vo CL, Park C, Lee BJ. Current trends and future perspectives of solid dispersions containing poorly water-soluble drugs. *Eur J Pharm Biopharm* 2013;85:799-813.
- Kawabata Y, Wada K, Nakatani M, Yamada S, Onoue S. Formulation design for poorly water-soluble drugs based on biopharmaceutics classification system: Basic approaches and practical applications. *Int J Pharm* 2011;420:1-0.
- Xu W, Riikonen J, Lehto VP. Mesoporous systems for poorly soluble drugs. *Int J Pharm* 2013;453:181-97.
- Kurtagic H, Memic M, Selovic A. Effect of particle size on the dissolution of glibenclamide. *Int J Pharm Pharm Sci* 2013;5:775-9.
- Savjani KT, Gajjar AK, Savjani JK. Drug solubility: Importance and enhancement techniques. *ISRN Pharm* 2012;2012:195727.
- O'Shea JP, Nagarsekar K, Wieber A, Witt V, Herbert E, O'Driscoll CM, *et al.* Mesoporous silica-based dosage forms improve bioavailability of poorly soluble drugs in pigs: Case example fenofibrate. *J Pharm Pharmacol* 2017;69:1284-92.
- Tahvanainen M, Rotko T, Mäkilä E, Santos HA, Neves D, Laaksonen T, *et al.* Tablet preformulations of indomethacin-loaded mesoporous silicon microparticles. *Int J Pharm* 2012;422:125-31.
- Van Speybroeck M, Mols R, Mellaerts R, Thi TD, Martens JA, Van Humbeeck J, *et al.* Combined use of ordered mesoporous silica and precipitation inhibitors for improved oral absorption of the poorly soluble weak base itraconazole. *Eur J Pharm Biopharm* 2010;75:354-65.
- Guzmán HR, Tawa M, Zhang Z, Ratanabanangkoon P, Shaw P, Gardner CR, *et al.* Combined use of crystalline salt forms and precipitation inhibitors to improve oral absorption of celecoxib from solid oral formulations. *J Pharm Sci* 2007;96:2686-702.
- Brouwers J, Brewster ME, Augustijns P. Supersaturating drug delivery systems: The answer to solubility-limited oral bioavailability? *J Pharm Sci* 2009;98:2549-72.
- Balaji A, Kumari MH. *In vitro* interaction studies between-lumefantrine and lamivudine/metonidazole. *Int J Pharm Ind Res* 2013;3:335-45.
- Ingle VP, Talele GS. Comparative effect of metformin in combination with glimepiride and glibenclamide on lipid profile in Indian patients with Type 2 diabetes mellitus. *Int J Pharm Pharm Sci* 2011;3:472-4.
- Nikghalb LA, Singh G, Singh G, Kahkeshan KF. Solid dispersion: Methods and polymers to increase the solubility of poorly soluble drugs. *J Appl Pharm Sci* 2012;2:170-5.
- Sambasevam KP, Mohamad S, Sarih NM. Synthesis and characterization of the inclusion complex of β -cyclodextrin and azomethine. *Int J Mol Sci* 2013;14:3671-82.
- McCarthy CA, Ahern RJ, Dontireddy R, Ryan KB, Crean AM. Mesoporous silica formulation strategies for drug dissolution enhancement: A review. *Expert Opin Drug Deliv* 2016;13:93-108.